

# Modelling the effect of ribosome mobility on the rate of protein synthesis

Olivier Dauloudet<sup>1,2,†</sup>, Izaak Neri<sup>3,†,\*</sup>, Jean-Charles Walter<sup>1,†,\*</sup>,

Jérôme Dorignac<sup>1</sup>, Frédéric Geniet<sup>1</sup>, Andrea Parmeggiani<sup>1,2\*</sup>

<sup>1</sup> *Laboratoire Charles Coulomb (L2C), Montpellier University, CNRS, Montpellier, France*

<sup>2</sup> *Laboratory of Parasite Host Interactions (LPHI),  
Montpellier University, CNRS, Montpellier, France*

<sup>3</sup> *Department of Mathematics, Kings College London, Strand, London, WC2R 2LS, UK and*

<sup>†</sup> *These authors contributed equally.*

(Dated: December 27, 2020)

Translation is one of the main steps in the synthesis of proteins. It consists of ribosomes that translate sequences of nucleotides encoded on mRNA into polypeptide sequences of amino acids. Ribosomes bound to mRNA move unidirectionally, while unbound ribosomes diffuse in the cytoplasm. It has been hypothesized that finite diffusion of ribosomes plays an important role in ribosome recycling and that mRNA circularization enhances the efficiency of translation, see e.g. Ref. [1]. In order to estimate the effect of cytoplasmic diffusion on the rate of translation, we consider a Totally Asymmetric Simple Exclusion Process (TASEP) coupled to a finite diffusive reservoir, which we call the Ribosome Transport model with Diffusion (RTD). In this model, we derive an analytical expression for the rate of protein synthesis as a function of the diffusion constant of ribosomes, which is corroborated with results from continuous-time Monte Carlo simulations. Using a wide range of biological relevant parameters, we conclude that diffusion in biological cells is fast enough so that it does not play a role in controlling the rate of translation initiation.

## I. INTRODUCTION

Cells synthesize proteins by first transcribing the hereditary information encoded in genes into functional mRNA, and subsequently by translating the mRNA nucleotide sequence into polypeptide sequences [1]. The translation of mRNA into a polypeptide sequence can be divided into three stages, namely, the initiation, elongation and termination stages [1]. During initiation, a ribosomal complex (consisting of two ribosomal subunits, initiation factors, and tRNA) is assembled at the 5' end of a mRNA chain. After initiation, the ribosomal complex moves (or elongates) from the 5' end towards the 3' end of the mRNA while forming a polypeptide chain. In the final termination stage, the ribosome complex releases the polypeptide chain, unbinds from the mRNA and disassembles.

Translation is mainly controlled at the initiation step, as it is the rate limiting step in translation [2–5]. Initiation is a complex process involving several molecular actors, and it is therefore difficult to understand all the molecular mechanisms that are relevant for translation control. Nevertheless, coarse-grained mathematical modelling can uncover which physical mechanisms play a role in translation control.

It has been argued that the recycling of ribosomes through Brownian diffusion in the cytosol plays an important role in the control or regulation of translation [1, 6–8]. When a ribosome unbinds from the mRNA after termination, it can either rebind to the same mRNA or bind to another mRNA. If the diffusion of ribosomes is slow enough, then circularization of the mRNA could enhance the rate of ribosome recycling through cytosolic diffusion [1, 6, 9, 10]. On the other hand, this effect would be negligible if diffusion of ribosomes is fast enough. In this paper we use physical modelling to determine whether recycling of ribosomes through diffusion can play a role in controlling mRNA translation.

In order to study how ribosome mobility affects the mRNA initiation rate and thus the protein production, we present a minimalistic physical model that describes both the translation of mRNA by ribosomes and the diffusion of ribosomes in the cytoplasm. We call this model the Ribosome Transport model with Diffusion (RTD). From a physical viewpoint, the RTD consists of particles (the ribosomes) that diffuse in a box and can bind to a one-dimensional substrate (mRNA). Particles bound to the substrate move unidirectionally and cannot overtake. The RTD consists thus in a Totally Asymmetric Simple Exclusion Process (TASEP) [11] in contact with a diffusive reservoir. If diffusion is fast enough, then we recover the standard TASEP model, which describes in detail the elongation stage of mRNA translation [12–15]. On the other hand, when diffusion is slow, then a concentration gradient is formed in the reservoir and there will be a tight coupling between active transport on the filament and diffusion in the reservoir. In this regime, the RTD describes the interplay of active and passive transport in cellular media, leading to the formation

---

\*Electronic address: izaak.neri@kcl.ac.uk; Electronic address: jean-charles.walter@umontpellier.fr; Electronic address: andrea.parmeggiani@umontpellier.fr

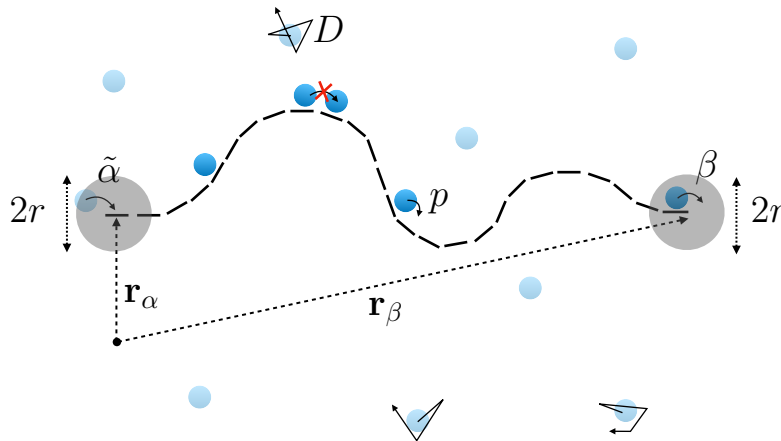


FIG. 1: *Graphical illustration of the Ribosome Transport with Diffusion model (RTD)*. The mRNA is represented with a dashed line, ribosomes processing along the mRNA at a rate  $p$  are represented by dark blue discs, and ribosomes diffusing freely at a diffusion coefficient  $D$  are represented by light blue discs. Grey discs of radius  $r$  centered at the end point of the mRNA are the reaction volumes: if a diffusing ribosome is located in the reaction volume at the mRNA end-point centred around position  $\mathbf{r}_\alpha$ , then it attaches at a rate  $\tilde{\alpha}$  to the mRNA. On the other hand, if a ribosome is at the last site of the mRNA, then it detaches at a rate  $\beta$  and is released inside the reaction volume centred around  $\mathbf{r}_\beta$ .

of a gradient of molecular species. Phenomena of active transport coupled to a diffusive reservoir have been studied before in the literature, see for example Refs. [6–8, 16–25, 35, 61]. In these studies, much focus has been put on nonequilibrium phase transitions [11, 21, 26, 27].

In the present paper, we use mean-field theory to derive an analytical expression for the protein synthesis in the RTD model, which is corroborated with numerical results obtained from continuous-time Monte Carlo simulations. Subsequently, we use the analytical expression for the protein synthesis rate to discuss the biological relevance of Brownian diffusion in ribosomal recycling. By considering a broad range of biological parameters, we come to the conclusion that under physiological conditions finite diffusion of ribosomes is not important in the control of mRNA translation. Thus, circularisation should not occur in order to prevent the limiting effect of Brownian diffusion of ribosomes in the cytoplasm on initiation of translation [1, 6, 9, 10]. In addition, we discuss how the spatial dimensions of the reservoir and geometry impact the protein synthesis rate and we find qualitative difference in the dependence of the protein synthesis rate on the length of the mRNA between two and three dimensions. Both cases are biologically relevant: the three-dimensional case applies to cytoplasmic translation, whereas the two-dimensional case applies to endoplasmic reticulum translation.

The paper is organized as follows. In Sec. II, we define the RTD model. In Sec. III, we present a mean-field theory for the RTD model and derive analytical expressions for the protein synthesis rate as a function of the diffusion coefficient of ribosomes. In Sec. IV, we compare theory with simulation results using a continuous-time algorithm. In Sec. V, we discuss the biological relevance of the model. We conclude the paper with a discussion in Sec. VI, and in Appendix A we present analytical results for the concentration profile of ribosomes in the cytoplasm.

## II. MODEL DEFINITION: RIBOSOME TRANSPORT WITH DIFFUSION

We introduce here the RTD, a minimalistic model that allows us to study how diffusion determines the rate of protein synthesis. The RTD consists of ribosomes that diffuse in a medium embedded in two or three dimensions and can bind to a one-dimensional substrate, say a mRNA filament. Bound ribosomes then move unidirectionally along the filament by converting the intracellular chemical energy from the hydrolysis of guanine triphosphate (GTP) into mechanical motion, which is modelled by a Totally Asymmetric Simple Exclusion Process (TASEP). In Fig. 1, we present an illustration of the model and its parameters.

We consider a filament immersed in a medium containing ribosomes at a concentration  $c_\infty$ . The filament is a monopolymer consisting of  $\ell$  monomers of length  $a$ . The first and last monomers of the filament are located at positions  $\mathbf{r}_\alpha$  and  $\mathbf{r}_\beta$ , respectively. For simplicity, we consider that  $\mathbf{r}_\alpha$  and  $\mathbf{r}_\beta$  are fixed in time.

The dynamics of unbound molecular motors is modelled as a Brownian motion with diffusion coefficient  $D$ .

The dynamics of bound molecular motors is a unidirectional, hopping process with excluded volume interactions,

which we model with a TASEP on a one-dimensional lattice of length  $L = \ell a$  [12, 13, 26, 27]. The TASEP model is a Markov jump process with the following rates: the hopping (or elongation) rate  $p$  at which particles make a step of length  $a$ , the exit rate  $\beta$  at which particles detach from the filament end-point, and the entry rate

$$\alpha(t) = \tilde{\alpha} N_r(t), \quad (1)$$

where  $\tilde{\alpha}$  is the rate at which ribosomes contained in the reaction volume bind to the filament and  $N_r(t)$  is the number of ribosomes present in the reaction volume at time  $t$ . The reaction volume is considered to be a sphere (in three dimensions) or a disc (in two dimensions) of radius  $r$  centered around the first monomer of the filament located at  $\mathbf{r}_\alpha$ . The reaction volume radius is of the same order of magnitude as the size of a ribosome. When ribosomes detach from the filament they appear at a random location in a sphere (in three dimensions) or disc (in two dimensions) of radius  $r$  centered around  $\mathbf{r}_\beta$ . Because of excluded volume interactions, each monomer can be bound to at most one ribosome. Therefore, ribosomes cannot hop forward if the subsequent monomer is already occupied by a ribosome and ribosomes cannot bind to the first monomer when it is already occupied, as illustrated in Fig. 1.

### III. MEAN-FIELD THEORY FOR COUPLING OF DIFFUSION WITH ACTIVE TRANSPORT

We present a mean field theory for the RTD model that couples diffusion with active transport. First, in Sec. III A, we discuss how the protein synthesis rate is related to the stationary current of the TASEP model. Second, in Sec. III B, we derive an analytical expression for the protein synthesis rate that is independent of the geometrical properties of the medium or reservoir in which the one-dimensional substrate is immersed. Lastly, in Sec. III C, we discuss the impact of the geometry of the surrounding reservoir on the protein synthesis rate.

#### A. Protein synthesis rate is given by the stationary current on the filament

The quantity of interest from a biological point of view is the protein synthesis rate  $J$ , which corresponds with the stationary current of particles on the filament [12, 13].

The stationary current of the RTD model in the limit of infinitely large  $D$  is equal to the stationary current  $\mathcal{J}$  of the TASEP model. In the limit of large  $\ell$ , it holds that [11, 26, 36]

$$\mathcal{J} = \begin{cases} \alpha \left(1 - \frac{\alpha}{p}\right), & \alpha < \beta \text{ and } \alpha < p/2, & \text{(LD)}, \\ \beta \left(1 - \frac{\beta}{p}\right), & \beta < \alpha \text{ and } \beta < p/2, & \text{(HD)}, \\ \frac{p}{4}, & \alpha \geq p/2 \text{ and } \beta \geq p/2, & \text{(MC)}. \end{cases} \quad (2)$$

The three branches in Eq. (2) correspond with three nonequilibrium phases: a Low-Density phase (LD) at small entry rates  $\alpha < \beta$  and  $\alpha < p/2$ , a High-Density phase (HD) at small exit rates  $\beta < \alpha$  and  $\beta < p/2$ , and a Maximal Current phase (MC) when both  $\alpha \geq p/2$  and  $\beta \geq p/2$ . In the LD phase, the ribosome attachment process is rate limiting and the current is a function of  $\alpha$ ; in the HD phase, the ribosome detachment process is rate limiting and the current is a function of  $\beta$ ; and in the MC phase, the filament hopping process is rate limiting and the current is independent of both  $\alpha$  and  $\beta$ . Experimental data in yeast cells [33] and in neurons of mammals [34] show that the rate limiting process for translation is the initiation of ribosomes.

In the RTD model at finite values of  $D$ , the entry rate  $\alpha(t)$  on the filament is not a constant but a fluctuating quantity, see Eq. (1). In the stationary state, the average current  $J$  is well approximated by the expression (2) with the entry rate  $\alpha$  replaced by its average value

$$\langle \alpha(t) \rangle = \tilde{\alpha} \langle N_r(t) \rangle, \quad (3)$$

where  $\langle \cdot \rangle$  denotes the average over many realizations of the stationary process. Since in the stationary state the average number  $\langle N_r(t) \rangle$  of ribosomes in the reaction volume is independent of time, we set

$$\langle \alpha(t) \rangle = \langle \alpha \rangle. \quad (4)$$

Replacing in Eq. (2)  $\alpha$  by  $\langle \alpha \rangle$ , which is a mean-field assumption, we obtain for the stationary current of the RTD model the expression

$$J = \begin{cases} \langle \alpha \rangle \left(1 - \frac{\langle \alpha \rangle}{p}\right), & \langle \alpha \rangle < \beta \text{ and } \langle \alpha \rangle < p/2, & \text{(LD)}, \\ \beta \left(1 - \frac{\beta}{p}\right), & \beta < \langle \alpha \rangle \text{ and } \beta < p/2, & \text{(HD)}, \\ \frac{p}{4}, & \langle \alpha \rangle \geq p/2 \text{ and } \beta \geq \frac{p}{2}, & \text{(MC)}. \end{cases} \quad (5)$$

From Eq. (5) we observe that if the filament is in the HD or MC phase, then the protein synthesis rate is independent of the diffusion process in the reservoir. However, in the LD phase when the initiation step is rate limiting, which is biologically relevant case, the current  $J$  depends on the concentration of unbound ribosomes through  $\langle\alpha\rangle$ , and hence in this regime we are required to include diffusion into our theoretical analysis. Often it will be insightful to consider the limiting case where particle excluded volume on the filament is irrelevant for which the simpler formula

$$J = \langle\alpha\rangle \quad (6)$$

holds. Note that this condition is fulfilled for low density of ribosomes on the filament.

### B. Protein synthesis rate: universal expression

From the point of view of the reservoir of diffusing ribosomes the filament serves both as a sink and a source of ribosomes.

If the initiation and termination sites overlap, as will be approximately the case for circular mRNA, then the concentration of ribosomes in the reservoir will be homogeneous since source and sink exactly compensate for each other, and therefore in this case

$$\langle\alpha\rangle = \alpha_\infty = \bar{\alpha}c_\infty\mathcal{V}, \quad (7)$$

where  $\mathcal{V}$  is the reaction volume of radius  $r$ , which for two dimensions and three dimensions is given by  $\mathcal{V} = \pi r^2$  and  $\mathcal{V} = 4\pi r^3/3$ , respectively.

On the other hand, if the termination site is distant from the initiation site, then  $\langle\alpha\rangle$  will have a reduced value, with respect to Eq. (7) due to the depletion of ribosomes in the reaction volume at the initiation site. Indeed, the current on the filament carries away ribosomes from the reaction volume, which in the stationary state will be compensated by the diffusive current in the reservoir. As we will show in the next section, the depletion effects due to finite diffusion are captured by the formula

$$\langle\alpha\rangle = \alpha_\infty \left(1 - \frac{J\mu_d}{D_{\text{eff}}\alpha_\infty}\right), \quad (8)$$

where  $\mu_d$  is a constant that depends on the geometry of the problem and where

$$D_{\text{eff}} = \frac{D}{\tilde{\alpha}r^2} \quad (9)$$

is an effective diffusion coefficient. The dimensionless quantity  $D_{\text{eff}}$  quantifies the competition between injection of ribosomes on the filament and the diffusion of ribosomes into the reaction volume. Equation (8) follows from solving the diffusion equation for ribosomes in the reservoir, as we shall describe in detail in the next section. Eq. (8) states that the rate  $\langle\alpha\rangle$  is the sum of the entry rate  $\alpha_\infty$  for a homogeneous reservoir minus a correction term that captures the effect of finite diffusion on the entry rate. The correction term is negative since the filament depletes particles in the reaction volume at the initiation site. Moreover, Eq. (8) states that the correction term is proportional to the current  $J$  on the filament, inversely proportional to the effective diffusion constant  $D_{\text{eff}}$ , and it is also proportional to the dimensionless, nonuniversal constant  $\mu_d$  that depends, as we shall see in the next section, on the geometrical properties of the system, namely, the end-to-end distance  $|\mathbf{r}_\beta - \mathbf{r}_\alpha|$ , the location of the filament in the reservoir, the dimensionality of the system, and the boundary conditions of the reservoir of diffusing ribosomes. Here, we would like to focus on the physical consequences of the Eq.(9).

To obtain the protein synthesis rate  $J$ , we combine Eqs. (5) and (8). In the LD phase, we obtain a second-order algebraic equation whose solution  $\langle\alpha\rangle \in [0, p/2]$  is given by

$$\langle\alpha\rangle = p \frac{D_{\text{eff}} + \mu_d}{2\mu_d} \left(1 - \sqrt{1 - 4\zeta}\right), \quad (10)$$

where the adimensional parameter

$$\zeta = \frac{\alpha_\infty D_{\text{eff}} \mu_d}{p(D_{\text{eff}} + \mu_d)^2} \quad (11)$$

quantifies the effect of exclusion on  $\langle\alpha\rangle$ . The argument of the square root in (10) is always positive when the filament is in the LD phase because in the LD phase  $\langle\alpha\rangle = p \frac{D_{\text{eff}} + \mu_d}{2\mu_d} < p/2$ , which implies  $\zeta < 1/4$ . Note that if the diffusion

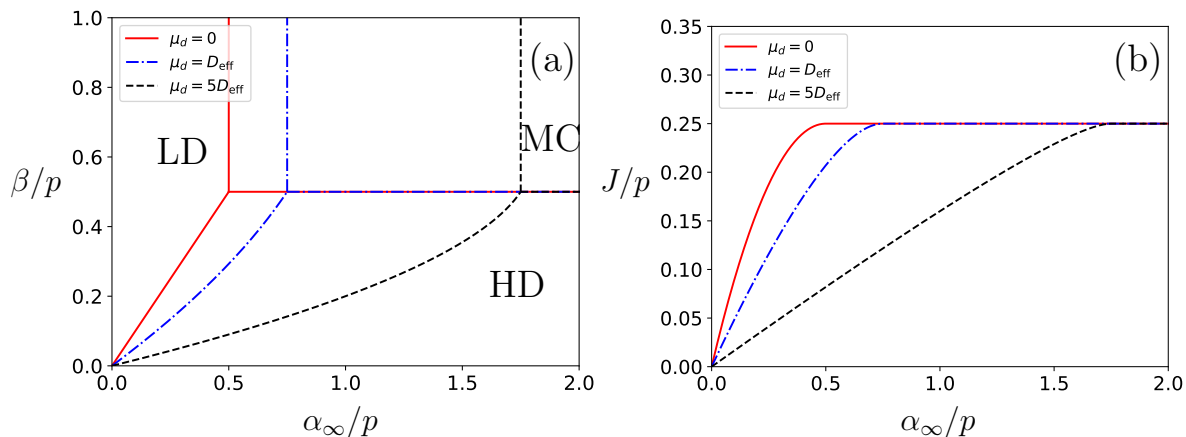


FIG. 2: Panel (a): phase diagram for the RTD model for three values of the parameter  $\mu_d/D_{\text{eff}}$ . Panel (b): protein synthesis rate  $J/p$  in the RTD model as a function of the ratio  $\alpha_\infty/p$  for a large exit rate  $\beta > p/2$ .

coefficient  $D_{\text{eff}}$  is small enough, then  $\zeta \ll 1$  and exclusion has a minor effect. Plugging  $\langle \alpha \rangle$  inside the expression for the current, given by Eq. (5), we obtain the following expression for the protein synthesis rate,

$$J = \begin{cases} \langle \alpha \rangle (1 - \langle \alpha \rangle / p), & \alpha_\infty < \beta \left[ 1 + \frac{\mu_d}{D_{\text{eff}}} (1 - \beta/p) \right] \text{ and } \alpha_\infty < p/2 \left( 1 + \frac{\mu_d}{2D_{\text{eff}}} \right), \quad (\text{LD}), \\ \beta \left( 1 - \frac{\beta}{p} \right), & \alpha_\infty > \beta \left[ 1 + \frac{\mu_d}{D_{\text{eff}}} (1 - \beta/p) \right] \text{ and } \beta < p/2, \quad (\text{HD}), \\ \frac{p}{4}, & \alpha_\infty \geq p/2 \left( 1 + \frac{\mu_d}{2D_{\text{eff}}} \right) \text{ and } \beta \geq p/2, \quad (\text{MC}), \end{cases} \quad (12)$$

where  $\langle \alpha \rangle$  is given by (10). For small values of  $\zeta$ , we obtain the simpler expression

$$J = \frac{\alpha_\infty D_{\text{eff}}}{D_{\text{eff}} + \mu_d}, \quad (13)$$

which also follows from Eq. (6). Equation (12) implies that the current  $J$  admits a universal expression that only depends on four parameters: the entry rate  $\alpha_\infty$  for a homogeneous reservoir, the elongation rate  $p$ , the exit rate  $\beta$ , and the parameter  $\mu_d/D_{\text{eff}}$  that quantifies the effect of finite diffusion on the current  $J$ . From Eqs.(12) and (13) it also follows that the effect of finite mobility of ribosomes on the protein synthesis rate  $J$  is significant when  $\mu_d \gg D_{\text{eff}}$ . On the other hand, when  $\mu_d \ll D_{\text{eff}}$ , then the finite mobility of ribosomes will be irrelevant for  $J$ .

In Fig. 2(a), we present the phase diagram for the RTD model for three values of  $\mu_d/D_{\text{eff}}$ , namely, the case with an infinite diffusion rate,  $\mu_d/D_{\text{eff}} = 0$ , and two cases with finite diffusion rates,  $\mu_d = D_{\text{eff}}$  and  $\mu_d = 5D_{\text{eff}}$ . For  $\mu_d/D_{\text{eff}} = 0$ , we recover the phase diagram of TASEP [11, 26, 36], while for finite values of  $\mu_d$  we observe an increase of the LD phase and a corresponding decrease of the MC and HD phases. This is because finite diffusion depletes particles in the reaction volume surrounding the initiation site of the filament, and hence reduces the current on the filament for a given  $\alpha_\infty$ . This is shown in Fig. 2(b), where we plot the current as a function of  $\alpha_\infty/p$  for fixed a value of  $\mu_d/D_{\text{eff}}$  and  $\beta/p \geq 1/2$ . If  $\mu_d \ll D_{\text{eff}}$ , then the reservoir is homogeneous and we obtain the standard TASEP result [11, 26, 36]

$$J = \begin{cases} \alpha_\infty (1 - \alpha_\infty / p), & \alpha_\infty < p/2, \\ p/4, & \alpha_\infty > p/2. \end{cases} \quad (14)$$

In the opposing limiting case when  $\mu_d \gg D_{\text{eff}}$  the reservoir is strongly inhomogeneous and we obtain that

$$J = \begin{cases} \frac{D_{\text{eff}} \alpha_\infty}{\mu_d}, & \alpha_\infty < p\mu_d/4, \\ p/4, & \alpha_\infty > p\mu_d/4. \end{cases} \quad (15)$$

In this limit the environment is viscous and therefore the effects of excluded volume become negligible.

Note that the results of Fig.2 do not consider the effects of finite resources. Therefore, it is implicitly assumed that the number of ribosomes is very large compared to the average number of ribosomes on the mRNA. In the case of finite resources, the phase diagram displays an extended shock phase, as shown in Refs. [35, 62].

So far, much of the interesting physics has been hidden in the dimensionless constant  $\mu_d$  that depends on the geometry of the problem. In the next subsection we will explicitly solve the diffusion equation coupled to directed transport on the filament to obtain explicit expressions for  $\mu_d$ .

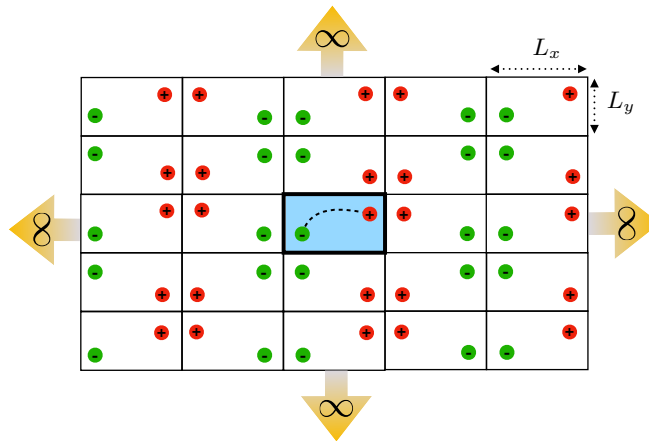


FIG. 3: *Illustration of the method of images*: Diffusion of ribosomes in a confined rectangular box is equivalent to diffusion of ribosomes in a two-dimensional Euclidean space that contains an infinite number of images of the original source (denoted by red) and sink (denoted by green) located in the rectangular box (located in the center and coloured in blue).

### C. Influence of geometry on the protein synthesis rate

In order to obtain an expression for  $\mu_d$ , and thus complete the theoretical treatment for ribosomes with finite mobility, we solve the diffusion equation in the reservoir coupled with active transport on the filament. We consider the case where  $|\mathbf{r}_\beta - \mathbf{r}_\alpha| > 2r$  so that the reaction volumes at the source and the sink do not overlap.

The stationary concentration of unbound ribosomes is described by the diffusion equation

$$D \Delta c(\mathbf{r}) = \Pi(\mathbf{r}), \quad (16)$$

where  $c(\mathbf{r})$  is the concentration of ribosomes at the spatial coordinate  $\mathbf{r} \in \mathbb{R}^d$ ,  $\Delta$  is the Laplacian with respect the radius  $\mathbf{r}$ , and

$$\Pi(\mathbf{r}) = \begin{cases} -\frac{J}{V} & |\mathbf{r} - \mathbf{r}_\alpha| \leq r, \\ \frac{J}{V} & |\mathbf{r} - \mathbf{r}_\beta| \leq r, \\ 0 & |\mathbf{r} - \mathbf{r}_\alpha| > r \quad \text{and} \quad |\mathbf{r} - \mathbf{r}_\beta| > r, \end{cases} \quad (17)$$

where we have used that  $|\mathbf{r}_\beta - \mathbf{r}_\alpha| > 2r$ .

The diffusion equation admits the solution

$$c(\mathbf{r}) = \int_{\mathbb{R}^d} d^d \mathbf{r}' \Pi(\mathbf{r}') \mathcal{G}_d(\mathbf{r}, \mathbf{r}'), \quad (18)$$

where  $\mathcal{G}(\mathbf{r}, \mathbf{r}')$  is the Green function that solves

$$D \Delta \mathcal{G}_d(\mathbf{r}, \mathbf{r}') = \delta(\mathbf{r} - \mathbf{r}'). \quad (19)$$

The entry rate  $\langle \alpha \rangle$  is related to the stationary concentration in the reaction volume through

$$\langle \alpha \rangle = \tilde{\alpha} \int_{|\mathbf{r} - \mathbf{r}_\alpha| \leq r} c(\mathbf{r}) d\mathbf{r}. \quad (20)$$

The explicit form of the Green's function and thus  $\langle \alpha \rangle$  depend on the geometry of the reservoir. We provide below a couple of examples.

#### 1. RTD in two-dimensional infinite box ( $\mathbb{R}^2$ )

In two dimensions, the Green function takes the form [56, 57]

$$\mathcal{G}_2(\mathbf{r}, \mathbf{r}') = -\frac{1}{2\pi} \ln |\mathbf{r} - \mathbf{r}'|. \quad (21)$$

Substituting the Green function in Eq. (18), we obtain an explicit expression for  $c(\mathbf{r})$ , see Appendix A. Subsequently, substituting the explicit solution for  $c(\mathbf{r})$  in Eq. (20) we obtain the formula Eq. (8) with

$$\mu_2 = \frac{\log d_{\alpha\beta} + 1}{2}, \quad (22)$$

where

$$d_{\alpha\beta} = \frac{|\mathbf{r}_\beta - \mathbf{r}_\alpha|}{r} \quad (23)$$

is the effective distance between the initiation site and the termination site on the filament. Substitution of  $\mu_d$  into Eqs. (10-12) provides us with an explicit expression for the current  $J$  as a function of  $d_{\alpha\beta}$ .

In Fig. 4, we plot the current  $J$  as a function of the separation  $d_{\alpha\beta}$  between the two end-points of the mRNA for two values of the effective diffusion constant  $D_{\text{eff}}$ . Although the part for  $d_{\alpha\beta} < 2$  is not covered by our calculations, we know that  $J = \alpha_\infty(1 - \alpha_\infty/p)$  for  $d_{\alpha\beta} = 0$ , which in Fig. 4 corresponds to  $J = 0.24p$ . We observe that the current decreases monotonically as function of  $d_{\alpha\beta}$  and approaches zero for  $d_{\alpha\beta}$  large enough. The decay towards zero is logarithmically slow after a fast initial decay in the regime  $d_{\alpha\beta} < 2$  where initiation and termination sites overlap.

### 2. RTD in three-dimensional infinite box ( $\mathbb{R}^3$ )

In three dimensions the Green function is given by

$$\mathcal{G}_3(\mathbf{r}, \mathbf{r}') = \frac{1}{4\pi} \frac{1}{|\mathbf{r} - \mathbf{r}'|}. \quad (24)$$

Using this expression for the Green function in Eq. (18), we obtain an explicit expression for  $c(\mathbf{r})$ , see Appendix A, which we substitute in Eq. (20) to obtain formula Eq. (8) with now

$$\mu_3 = \frac{2}{5} - \frac{1}{3d_{\alpha\beta}}. \quad (25)$$

Comparing Eqs. (22) and (25), we see that there is a difference between two and three dimensions: in three dimensions  $\mu_3$  converges to a finite value for  $d_{\alpha\beta} \rightarrow \infty$  whereas in two dimensions  $\mu_2$  diverges for  $d_{\alpha\beta} \rightarrow \infty$ . This implies that in two dimensions  $J$  converges to zero for large distances  $d_{\alpha\beta}$  between the end-points of the filament, while it converges to a finite nonzero value in three dimensions.

The distinction between the dependency of the current  $J$  in two and three dimensions is illustrated in Fig. 4. In three dimensions, the current saturates fast to its asymptotic value after an initial quick decay for values  $d_{\alpha\beta} < 2$ . The asymptotic value of  $J$  depends on the diffusion constant  $D_{\text{eff}}$  and decreases to zero for  $D_{\text{eff}} \rightarrow 0$ . Hence, in three dimensions, the mRNA will carry a finite current, even when  $d_{\alpha\beta} \rightarrow \infty$ , and this asymptotic current will depend on the diffusion constant.

In Fig. 5, we plot the asymptotic current  $J$  as a function of the effective diffusion constant  $D_{\text{eff}}$ . We observe from Fig. 5 that at finite  $D_{\text{eff}}$  the protein synthesis rate in  $d = 2$  dimensions is smaller than the synthesis rate in  $d = 3$  dimensions. This is because diffusive currents are smaller in lower dimensions and hence ribosomes are more depleted at the filament entrance. For small values of  $D_{\text{eff}}$ , the current is proportional to  $D_{\text{eff}}$ , namely,

$$J = \frac{\alpha_\infty}{\mu_d} D_{\text{eff}} + O(D_{\text{eff}}^2), \quad (26)$$

where the proportionality constant is the ratio between the entry rate  $\alpha_\infty$  for circularized mRNA and the constant  $\mu_d$  that depends on the geometry of the problem.

### 3. Two-dimensional rectangular box

We consider the case of a filament immersed into a medium that has the shape of a two-dimensional rectangular box. We assume that the box is centered at the origin  $\mathbf{r} = 0$  and that the sides of the box have lengths  $L_x$  and  $L_y$ .

We derive an explicit expression for the Green function in a two-dimensional rectangular box with the method of images [58]. The Green function of a point source in a two-dimensional rectangular box is identical to a series of Green functions in  $\mathbb{R}^2$  associated with images of the point source, namely, it holds that

$$\mathcal{G}_{L_x, L_y}(\mathbf{r}, \mathbf{r}') = \mathcal{G}_2(\mathbf{r}, \mathbf{r}') + \sum_{j \in \mathcal{N}} \mathcal{G}_2(\mathbf{r}, \mathbf{r}^{(j)}), \quad (27)$$

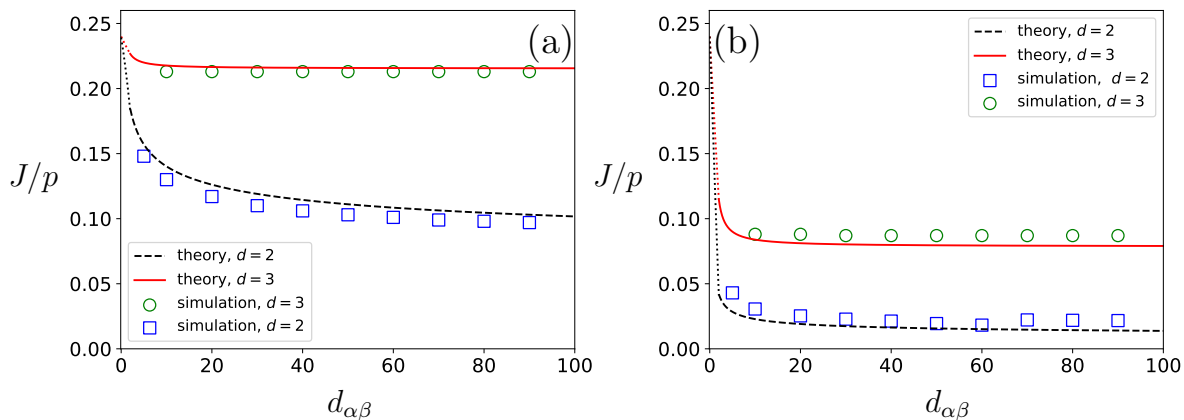


FIG. 4: Protein synthesis rate  $J/p$  as a function of the filament end-to-end distance  $d_{\alpha\beta}$  for parameters  $\alpha_{\infty}/p = 0.4$ ,  $\beta/p = 1$  for  $D_{\text{eff}} = 1$  [Panel(a)] and  $D_{\text{eff}} = 0.1$  [Panel (b)]. Theoretical result Eq. (12) for filaments in  $\mathbb{R}^2$  ( $d = 2$ , red solid lines) and  $\mathbb{R}^3$  ( $d = 3$ , black dashed lines) are compared with simulations results for filaments consisting of  $\ell = 100$  monomers (markers). The theoretical result Eq. (12) applies for  $d_{\alpha\beta} > 2$  and  $J = 0.24$  for  $d_{\alpha\beta} = 0$ . Therefore, we have added dotted lines connecting  $J = 0.24$  for  $d_{\alpha\beta} = 0$  with  $J$  at  $d_{\alpha\beta} = 2$ . The remaining parameters that specify the simulations can be found in Sec. IV.

where  $\mathbf{r}^{(j)}$  are the coordinates for the images of the point source located at  $\mathbf{r}'$ , see Fig. 3 for an example, and  $\mathcal{G}_2$  is the Green function in Eq. (21).

Substituting the Green function given by Eq. (27) in Eq. (20), we obtain the expression Eq. (8), with now

$$\mu_2(L_x, L_y) = \frac{1 + \log d_{\alpha\beta} + \mathcal{I}_{L_x, L_y}}{2}, \quad (28)$$

and where  $\mathcal{I}_{L_x, L_y}$  is the series

$$\mathcal{I}_{L_x, L_y} = \sum_{j \in \mathcal{N}_{\beta}} \log |\mathbf{r}_{\alpha} - \mathbf{r}_{\beta}^{(j)}| - \sum_{j \in \mathcal{N}_{\alpha}} \log |\mathbf{r}_{\alpha} - \mathbf{r}_{\alpha}^{(j)}|. \quad (29)$$

The sums in Eq. (29) run over the images of the initiation and termination sites of the filament, which defines the set  $\mathcal{N}_{\alpha}$  and  $\mathcal{N}_{\beta}$ . The specific locations of  $\mathbf{r}_{\alpha}^{(j)}$  and  $\mathbf{r}_{\beta}^{(j)}$  are detailed in Fig. 3. As shown in Ref. [35], the series Eq. (29) converges rapidly since the influence of the copies  $\mathbf{r}_{\alpha}^{(j)}$  and  $\mathbf{r}_{\beta}^{(j)}$  on the concentration of ribosomes in the original system decreases fast enough with the distance.

Lastly, we note that the method of images works for a rectangular shaped box since two-dimensional Euclidean space can be tiled with rectangles. Other geometrical shapes that allow for a complete tiling of space are triangles and hexagons, see [35] and references therein.

#### 4. Three-dimensional cuboid

An analytical expression for the protein synthesis rate can also be derived in the case of a three-dimensional cuboid with linear dimensions  $L_x$ ,  $L_y$  and  $L_z$ . We then obtain formula Eq. (8) with

$$\mu_3(L_x, L_y, L_z) = \frac{2}{5} - \frac{1}{3} \left( \frac{1}{d_{\alpha\beta}} + \mathcal{I}_{L_x, L_y, L_z} \right) \quad (30)$$

where  $\mathcal{I}_{L_x, L_y, L_z}$  is the series

$$\mathcal{I}_{L_x, L_y, L_z} = \sum_{j \in \mathcal{N}_{\beta}} \frac{1}{|\mathbf{r}_{\alpha} - \mathbf{r}_{\beta}^{(j)}|} - \sum_{j \in \mathcal{N}_{\alpha}} \frac{1}{|\mathbf{r}_{\alpha} - \mathbf{r}_{\alpha}^{(j)}|}. \quad (31)$$

The sums run over the images of the initiation and termination sites of the filament in  $\mathbb{R}^3$ . For more in-depth analysis of the finite volume effects, see Ref. [35].



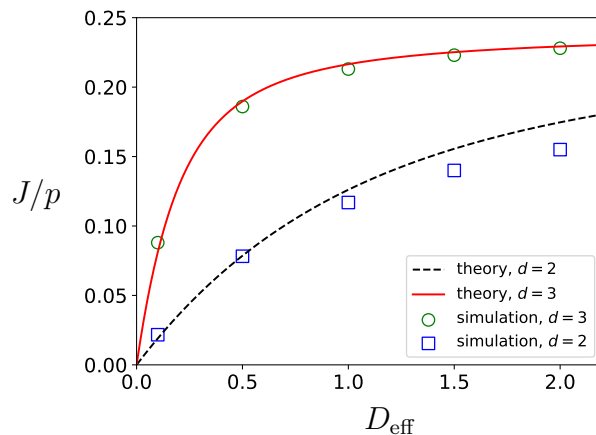


FIG. 5: Protein synthesis rate  $J/p$  as a function of the effective diffusion constant  $D_{\text{eff}}$  for filaments in  $\mathbb{R}^2$  ( $d = 2$ ) and  $\mathbb{R}^3$  ( $d = 3$ ). Analytical results from mean-field theory [solid lines depicting Eq. (12) with  $\mu_d$  as in Eqs. (22) or (25)] are compared with simulation results (circles). The parameters used to compute the theoretical curves are  $d_{\alpha\beta} = 20$ ,  $\alpha_{\infty}/p = 0.4$ , and  $\beta/p > 1/2$  (and therefore  $\lim_{D_{\text{eff}} \rightarrow \infty} J/p = 0.24$ ). The remaining parameters that specify the simulations can be found in Sec. IV.

#### IV. COMPARING MEAN-FIELD THEORY WITH SIMULATIONS

We have performed numerical simulations of the RTD to check the mean field assumptions in Eq.(5), as shown in Figs. 4 and 5. Theory and simulations are in very good correspondence, despite the fact that theory neglects correlations between particles, finite size effects on the filament due to boundary layers, and finite size effects due to the finite volume of the reservoir. The very good correspondence between numerical experiments and theory demonstrates that the expression for the current  $J$  given by Eqs. (10-12) is useful to quantify how finite mobility affects the protein synthesis rate  $J$ .

In what follows, we detail the specifics of the Monte Carlo simulations. Both components of the RTD, i.e., diffusion of particles and the active transport on the filament, can be simulated independently using a continuous-time Monte Carlo simulation on the TASEP [54, 55] and a Brownian motion in the reservoir. However, in order to simulate the RTD model, we need to couple the dynamics of the two processes.

##### A. Monte Carlo simulations of the RTD

In this subsection, we describe the algorithm used to simulate the dynamics of ribosome (i) in the reservoir, (ii) on the filament and (iii) how these two subsystems are coupled at the first and last site of the filament where the ribosomes respectively enter on and exit from the filament.

First, we detail the simulations of the unbound ribosomes diffusing in the reservoir. We consider that unbound ribosomes do not interact with each other and their position  $\vec{r}$  evolves according to a Brownian equation of motion

$$\frac{d\vec{r}}{dt} = \vec{\xi}(t), \quad (32)$$

where  $\vec{\xi}$  is a white noise such that

$$\langle \xi_a(t) \rangle = 0, \quad (33)$$

$$\langle \xi_a(t) \cdot \xi_b(t') \rangle = 2D\delta(t-t')\delta_{a,b}, \quad (34)$$

where the indices  $a$  and  $b$  stand for the space coordinates, i.e.,  $x$  and  $y$  for a two-dimensional reservoir;  $x$ ,  $y$  and  $z$  for three-dimensional reservoir. We integrate these equations numerically by discretizing time into intervals of length  $\Delta t = t - t'$ , such that

$$\frac{\vec{r}(t + \Delta t) - \vec{r}(t)}{\Delta t} = \vec{\xi}(t). \quad (35)$$

The  $\delta(t-t')$  in the amplitudes of the white noise are replaced by  $1/\Delta t$ , leading to the following update for each space component

$$r_a(t + \Delta t) = r_a(t) + \sqrt{2D\Delta t}\xi_a, \quad (36)$$

Second, we detail the simulations of ribosomes bound to a filament located inside the reservoir. The filament contains  $\ell$  sites and each site has the length  $r$  of a ribosome. The filament has thus a total length  $L = \ell r$ . The dynamics on the TASEP is performed with a continuous-time Monte Carlo algorithm [54, 55], sometimes called Gillespie algorithm [53]. The current configuration of ribosomes on the filament allows only a finite number of moves of ribosomes each given by the TASEP rules described above. For illustration, in the particular case of Fig.1, the first site is empty, thus a ribosome can enter at a rate  $\alpha = \tilde{\alpha}N(t)$ ; three ribosomes are present in the bulk of the filament without another ribosomes on their right side, thus they can jump to the right at a rate  $p$ ; and finally a ribosome occupies the exit site of the filament, so it can leave at the rate  $\beta$  the filament and return to the reservoir to resume a Brownian motion. It is useful to define the sum  $S_r$  of the possible transition rates; in the case of Fig.1,  $S_r = \alpha + \beta + 3p$ . A particular move is chosen with a probability linearly related to its rate and the filament is forced to perform this move. For instance, the probability  $P_\beta$  to move the ribosome from the exit site to the reservoir is  $P_\beta = \beta/S_r$ . This algorithm thus avoid rejection of ribosome moves, which spares a lot of computational time in the case of low and high densities of ribosomes, compared to a sequential algorithm. Indeed, a sequential algorithm consists in choosing randomly a site of the filament. This site is likely empty in the LD phase or stuck into a jam in the HD phase, leading in both cases to frequent rejections of the move trial. The other advantage of a continuous-time Monte Carlo is that the time of evolution of the filament during this move is explicitly defined from the transition rates like  $\tau \sim S_r^{-1}$ , and can thus take continuous values. The explicit definition of  $\tau$  will be useful to couple the time scale of the dynamics between the ribosomes on the filament and the ribosomes performing Brownian motion in the reservoir. Note that, intuitively, the sum of rate  $S_r$ , and thus the time  $\tau$  spent by the filament during a move both depend on the configuration of ribosomes. If  $S_r$  is small (large), i.e., if a transition is unlikely (resp. likely) to happen, then the time evolution of the filament will be large (resp. small).

Third, we discuss how the dynamics in the reservoir is coupled to transport on the filament. First we draw a time  $\tau$  from the continuous-time Monte Carlo algorithm, then update the reservoir configuration over this time by integrating the Brownian equations for each particle in the reservoir over the time  $\tau$ , and then draw another time  $\tau$  and so on. Hence, in this approach, we assume that in the time  $\tau$  the reservoir does not change significantly. The internal dynamics of ribosome hopping is by definition not coupled to the reservoir as, in the RTD the ribosomes can neither attach nor detach in the bulk of the filament. The coupling between reservoir and filament takes place at the first and last site of the filament. Therefore, it is sufficient to define the positions  $\mathbf{r}_\alpha$  and  $\mathbf{r}_\beta$  of the first and the last sites, respectively. Note that the total length  $L$ , which may however be different than the end-to-end distance  $d_{\alpha\beta} = |\mathbf{r}_\beta - \mathbf{r}_\alpha|$ , which can take any value between 0 and  $L$  depending on the conformation of the filament. Among the possible moves accounted in the simulation is the attachment of a ribosome at the entrance: we define a spherical reaction volume  $\mathcal{V}_\alpha = 4/3\pi r^3$  of radius  $r$  centered at the first site of the TASEP. If a ribosome in the reservoir is present in  $\mathcal{V}_\alpha$  and if the first site is empty, then it can attach at a rate  $\tilde{\alpha}$  (define in Eq.(1)). In the same way, a spherical volume  $V_\beta$  of radius  $r$  is centered at the exit site of the filament. If a ribosome exits the filament at a rate  $\beta$ , then it is released at a random position inside  $V_\beta$  and resumes a Brownian motion in the reservoir. Note that we have used the same numerical technique successfully in Ref. [19] to coupled the TASEP-LK with Brownian particles inside a reservoir.

## B. Parameters of the simulations

We describe in this paragraph the geometry of the simulated RTD. First, the filament is chosen to have a total contour length  $L = \ell r$  with  $\ell = 100$ , which is enough to keep boundary effects on the TASEP of the order of a few percents on the exact current, i.e., of the order of statistical fluctuations [59, 60]. In the simulations, the filament is located in the middle of the reservoir to ensure isotropy of the particle concentration and limiting boundary effects.

Second, the reservoir is chosen to be large with respect to  $d_{\alpha,\beta}$ . In three dimensions, we choose the dimensions  $L_x = L_y = 100 r$  in the orthogonal direction to the end-to-end distance, whereas the longitudinal direction to  $d_{\alpha,\beta}$  is taken to be larger, i.e.,  $L_z = 200 r$ . In two dimensions, we choose  $L_x = 400 r$  in the longitudinal direction and  $L_y = 200 r$  in the orthogonal direction. Note that the gradient of ribosomes in the reservoir induced by the transport on the filament is expected to be larger along the longitudinal direction to  $d_{\alpha,\beta}$ . This is why this dimension is chosen larger than the orthogonal directions. With these reservoir dimensions, boundary effects are small as the system is large with respect to the gradient of particles. The reflecting boundary conditions are implemented as follows: if the update of a Brownian particle leads to a position outside of the box, the move is rejected.

We now discuss the remaining parameters of the system linked to the concentration of ribosomes, attachment rate at the entry site of the filament and the diffusion coefficient of the Brownian motion. In three dimensions, we choose to include  $10^5$  ribosomes in the reservoir, leading to a density of ribosomes  $c_\infty = 0.05 r^{-3}$ ; whereas in two dimensions, we choose  $5 \cdot 10^5$  ribosomes in the system, leading to a density  $6.25 r^{-2}$ . In two and three dimensions, we choose  $\tilde{\alpha} = 0.4/c_\infty$ , so that  $\alpha_\infty = \tilde{\alpha} c_\infty = 0.4$  and  $D = 0.1\tilde{\alpha}r^2$  and  $D = \tilde{\alpha}r^2$  in Fig.3(a) and (b), so that  $D_{\text{eff}} = D/(\tilde{\alpha}r^2) = 0.1$  and 1, respectively. Finally, we chose  $\beta = p = 1$  like the analytical calculation, i.e., all rates

can be seen to be expressed in unit of  $p$ .

In this paragraph, we discuss how we choose correlation and equilibration time to increase the quality of the sampling during Monte Carlo simulations. The correlation time can be approximated by the time needed to replace all the ribosomes on the TASEP. During one MC iteration, the time spent during the update is  $\tau \sim 1/S_r \sim 1/(\rho\ell p)$  where  $\rho$  is the global density of ribosomes on the filament, i.e.,  $\rho = N_r/\ell$  where  $N_r$  is the total number of ribosomes on the filament. Note that, in the last approximation of  $\tau$ , the sum of the rates  $S_r$  is obtained assuming that it is dominated by the hopping rates in the bulk of the TASEP, which contains  $\approx \rho\ell$  particles. The last ribosome that entered the TASEP will need at least to be chosen  $\ell$  times amongst  $\rho\ell$  possibilities of moves. Therefore the correlation time becomes  $\tau_c \approx \rho\ell^2\tau = \ell/p$ . As  $p = 1$  and  $\ell = 100$  in our simulations (both two and three dimensions), we use  $\tau_c = 100$ . Starting with an empty initial configuration, we ensure the steady state by performing  $100\tau_c = 10^4$  iterations described above (continuous time on the filament and integration of the Brownian motion in the reservoir). Subsequently,  $2.10^4$  samplings are in three dimensions and  $10^5$  samplings in two dimensions, each spaced by  $\tau_c = 100$  iterations to decorrelate the configurations.

## V. BIOLOGICAL RELEVANCE OF DIFFUSION IN RIBOSOMAL RECYCLING

To determine the biological relevance of finite mobility for ribosomal recycling, we use experimentally measured values for the parameters that appear in the theoretical expression for the protein synthesis rate derived in Sec. III. We focus on two organisms for which the required microscopic parameters have been measured experimentally, namely, the bacterium *Escherichia coli* and the budding yeast *Saccharomyces cerevisiae*. Moreover, we focus on the three-dimensional case corresponding to cytoplasmic translation.

TABLE I: Impact of finite mobilities on ribosomal recycling in two organisms.

| <i>E. coli</i>                | <i>S. cerevisiae</i>           |
|-------------------------------|--------------------------------|
| $\mu_3/D_{\text{eff}} < 0.06$ | $\mu_3/D_{\text{eff}} < 0.007$ |

Since for physiological parameters the initiation of translation is the rate limiting step, we use the expression for the protein synthesis rate given by Eq. (13). Eq. (13) implies that if

$$\mu_d \ll D_{\text{eff}} \quad (37)$$

then diffusion has no meaningful influence on the protein synthesis rate. On the other hand, when

$$\mu_d \gg D_{\text{eff}} \quad (38)$$

then the influence of finite diffusion on protein synthesis rate is sizeable. Hence, in what follows we estimate the parameters  $\mu_d$  and  $D_{\text{eff}}$ .

### A. Estimate of $\mu_3$

First, we estimate the geometric parameter  $\mu_3$  corresponding to cytoplasmic translation. Formula (25), implies for a three dimensional and infinitely large reservoir that

$$\mu_3 \leq \frac{2}{5}, \quad (39)$$

where the equality is achieved in the limit  $d_{\alpha\beta} \rightarrow \infty$ .

### B. Estimate for $D_{\text{eff}}$ in *Escherichia coli*

In order to estimate  $D_{\text{eff}}$ , it is useful to rewrite the expression Eq. (9) in terms of  $\langle\alpha\rangle$ , which gives

$$D_{\text{eff}} = \frac{D\langle N_r \rangle}{\langle\alpha\rangle r^2} = \frac{4\pi Dc_u r}{3 \langle\alpha\rangle}, \quad (40)$$

where  $c_u$  is the concentration of unbound ribosomes. The quantity  $\langle\alpha\rangle$  is hard to estimate since it can vary in several orders of magnitude from one mRNA transcript to another, see for instance Ref. [5]. However, since initiation is the rate limiting step, it holds that

$$\langle\alpha\rangle < \frac{p}{2}, \quad (41)$$

with the elongation rate  $p$  being fairly independent of the mRNA transcript and the biological organism under study. Combining Eqs. (40) and (41), we obtain the lower bound

$$D_{\text{eff}} > \frac{8\pi D c_u r}{3 p}. \quad (42)$$

We are left to estimate the parameters  $D$ ,  $c_u$ ,  $r$  and  $p$ . We first consider the case of the bacteria *Escherichia coli*.

Empirical values for the diffusion of ribosomes in *E. coli* show that  $D \approx 0.04\mu\text{m}^2/\text{s}$ , see Table 4-1 in Ref. [37]. However, the diffusion coefficient of the subunits of unbound ribosomes (i.e., those not bound to mRNA), is one order of magnitude larger and given by  $D \approx 0.2\mu\text{m}^2/\text{s}$ , as shown in Ref. [43].

For the radius of the reaction volume  $r$ , we use that the reaction volume cannot be smaller than the radius of a ribosome (or one of its subunits), and thus  $r > 10\text{nm}$ , see Figure 1-40 in Ref. [37].

For *E. coli*, the elongation rate  $p$  has been measured in several experiments, see Refs. [44–46], leading to a value  $p$  of about about 10 – 20 codons per second. Since a ribosome occupies three codons, we take for  $p \approx 7\text{s}^{-1}$ .

Lastly, we need an estimate for the concentration

$$c_u = \frac{N_u}{V}. \quad (43)$$

The volume of *E. coli* is  $V \approx 1\mu\text{m}^3$  and its total number of ribosomes is about  $N_{\text{tot}} = 20000$  [37]. The fraction of unbound (or free) ribosomes is about 15% [43, 47] of the total value, leading to

$$c_u \approx 2 \times 0.15 \times 10^4 \mu\text{m}^{-3} \approx 3 \times 10^3 \mu\text{m}^{-3}. \quad (44)$$

Combining all parameter values into the right hand side of the bound Eq. (42) for  $D_{\text{eff}}$ , we obtain that

$$D_{\text{eff}} > \frac{8\pi}{3} \frac{0.2 \times 10 \times 3 \times 10^3 \text{ nm}}{7} \frac{\text{nm}}{\mu\text{m}} \approx 7.2, \quad (45)$$

and therefore

$$\frac{\mu_3}{D_{\text{eff}}} < 0.06. \quad (46)$$

We can conclude that diffusion has no sizeable effect on protein synthesis rates. This is in particular true since we have been very generous with all the biological parameters. For example, taking  $\langle\alpha\rangle < p/20$  instead of  $p/2$ , as in Ref. [48], would provide an even smaller upper bound  $\frac{\mu_3}{D_{\text{eff}}} < 0.006$ .

### C. Estimate for $D_{\text{eff}}$ in *Saccharomyces cerevisiae*

As a second example, we consider the case of budding yeast. We use again Eq. (42) to bound  $D_{\text{eff}}$ . All empirical values are known for this organism, see for instance table S1 in Ref. [5].

Empirical values for the diffusion coefficient of the 60S subunit of ribosomes in the dense nucleoplasm of budding yeast show that  $D \approx 0.3(\mu\text{m})^2/\text{s}$  [49]. We may expect that ribosomes diffuse faster in the cytoplasm, where translation takes place.

For the radius of the reaction volume  $r$ , we use again the reaction volume cannot be smaller than the radius of the ribosome, and thus  $r > 10\text{nm}$ .

The elongation rate of ribosomes in budding yeast has been measured to be  $p \sim 10$  codons per second and therefore  $p \approx 3\text{s}^{-1}$  since a ribosome occupies three codons [5, 50].

Finally, we come to the estimate of  $c_u$ , given by Eq. (43). The volume of a budding yeast cell is about  $V \approx 42\mu\text{m}^3$  [5, 51] and the number of ribosomes is  $2 \times 10^5$  [5, 30, 52]. Using again that a fraction 15% of ribosomes are unbound, see Figure 3 in [5], we obtain

$$c_u \approx \frac{2 \times 0.15 \times 10^5}{42} \mu\text{m}^{-3} \approx 7 \times 10^3 \mu\text{m}^{-3}, \quad (47)$$

which is in fact close to the concentration of unbound ribosomes in *E. coli*, see Eq. (44).

Combining all parameters in the bound given by Eq. (42), we obtain that

$$D_{\text{eff}} > \frac{8\pi}{3} \frac{0.3 \times 10 \times 7 \times 10^3 \text{ nm}}{3 \mu\text{m}} \approx 59 \quad (48)$$

and

$$\frac{\mu_3}{D_{\text{eff}}} < 0.007. \quad (49)$$

We should again bear in mind that the bound in Eq. (49) is a generous upper bound based on the bound on the initiation rates given by Eq. (41), and it is thus likely a loose bound and a significant overestimate for  $\mu_3/D_{\text{eff}}$ .

## VI. DISCUSSION

We have made a study of a totally asymmetric simple exclusion process immersed in a diffusive reservoir [11, 26], which we have called the RTD model. The RTD is a model for translation based on directed transport of ribosomes along mRNA and recycling of ribosomes through diffusion in the cytoplasm. We have used this model to determine whether under physiological conditions finite diffusion is a limiting factor for ribosome recycling.

We have derived an analytical expression for the current  $J$  at which mRNA is translated into proteins, which is corroborated by numerical simulation results. These results show that finite diffusion leads to a reduction in the translation rate  $J$  because the concentration of ribosomes at the mRNA initiation site is depleted. In addition, we find that the ratio between a geometric parameter  $\mu_d$  and an effective diffusion coefficient  $D_{\text{eff}}$  determines whether diffusion has an impact on the protein synthesis rate: if  $\mu_d \ll D_{\text{eff}}$ , then the concentration of ribosomes at the 5' end of the mRNA is not affected by finite diffusion; on the other hand, if  $\mu_d \gg D_{\text{eff}}$  then depletion of ribosomes at the mRNA initiation site is significant.

Using a broad range of physical parameters, we find that it is unlikely that finite diffusion is a limiting factor under physiological conditions in ribosome recycling. Indeed, in Table I, we present generous upper bounds for the parameter  $\mu_d/D_{\text{eff}}$  for two organisms, namely, the bacterium *E. coli* and the yeast *S. cerevisiae*. In both cases, we obtain that  $\mu_d/D_{\text{eff}}$  is substantially smaller than 1.

The outcome of our analysis, namely that the finite mobility of ribosomes does not play a role in translation control, is not a complete surprise, given that ribosomes diffuse at large enough rates. For example, it takes 0.1 s for a protein to diffuse across an *E. coli* cell and 10 s for a protein to diffuse across a yeast cell [39], while the time to translate a protein is about 2 min [39]. Hence, as much as concerns the translation of mRNA into proteins, the diffusion rate of ribosomes can be considered very large and therefore of negligible effect on the whole translation process. Also, since ribosome biogenesis is one of the most resource expensive process for the cell [29, 30], it is reasonable to assume that the molecular conditions are optimised by evolutionary constraints in order to render translation efficient, which in the present context implies that translation is not limited by ribosome mobilities.

From a biological point of view, these results imply that mRNA circularisation [1, 9] is not due to optimizing the recycling of ribosomes through diffusion in the cytoplasm. Instead, the circularisation of mRNA may regulate the efficiency of translation initiation through the binding strength of initiation factors to the mRNA [9, 10]. Hence, we come to a different conclusion than Ref. [7], which argues that three-dimensional diffusion of ribosomes in the cytoplasm plays an important role for mRNA translation control. Note that the question of the effect of the finite mobility of ribosomes on the current on mRNA remains open in two dimensions, as the diffusion coefficient of ribosomes constrained to a two-dimensional diffusion on the endoplasmic reticulum is not known to our knowledge.

Although finite diffusion is not limiting for ribosome recycling under physiological conditions, the RTD model may be relevant to explain the reduction in protein production when cells are in a dormant state. The mobility of cytoplasmic particles in dormant yeast cells is much lower than their mobility in yeast cells under normal conditions [31, 32]. The reduction in mobility of cytoplasmic particles is due to a transition between a fluid-like to a solid-like phase of the cytoplasm, which is triggered by the acidification of the cytosol [32]. The formula  $J \sim D$  indicates that the protein synthesis rate will scale proportional to the particle mobility.

The RTD model is also interesting as a model for the coupling between active transport and passive diffusion. Remarkably, the rate  $J$  admits a universal form that depends on five parameters only: the elongation rate  $p$ , the ratio  $\beta/p$  between the rate  $\beta$  of termination and  $p$ , the ratio  $\alpha_\infty/p$  between the initiation rate  $\alpha_\infty$  for a homogeneous reservoir (i.e., the limit of an infinitively fast diffusion) and  $p$ , an effective diffusion constant  $D_{\text{eff}}$ , and a dimensionless parameter  $\mu_d$  that quantifies the effect of the geometry of the reservoir and the filament on the current  $J$ . We have also found an interesting qualitative distinction between finite diffusion in two and three dimensions. In two dimensions, it holds that the current  $J$  vanishes in the large distance (between sink and source) limit, while in three dimensions

this limit gives a finite current  $J$ . However, the decay towards zero of  $J$  in two dimensions, which may be relevant for the endoplasmic reticulum translation, is logarithmically slow.

We end the paper by discussing the assumptions made by the RTD model and interesting future extensions of the present paper. First, we have ignored the fact that ribosomes disassemble into two subunits in the cytoplasm [1]. Hence, in principle we should consider a reservoir with two types of particles. However, if the mRNA binding rate one of these subunits is rate limiting, then the predictions of our model would remain valid. Interestingly, experimental data indicates that in prokaryotes the binding of the 40S ribosomal subunit is thought to be the rate-limiting step of initiation [4]. Second, we have assumed that mRNA has zero mobility and we have also assumed that the endpoints of the mRNA are immobile. However, including diffusion of the mRNA in the model would not alter the main conclusions of this paper, since it would only reduce the effects of finite diffusion on the protein synthesis rate. Third, it is known that cytoplasmic particles diffuse anomalously within living cells [40–42] and therefore a model based on fractional Brownian motion is more appropriate [42]. However, the exponent of the anomalous diffusion is close to 1 (0.88 for nanosilica particles of various sizes in yeast cells [32]), and therefore we expect it not to have a major impact on short length scales. It would nevertheless be interesting to analyse the dependence of  $J$  on  $d_{\alpha\beta}$  in this case.

### Acknowledgments

This work was supported in part by a Modélisation pour le Vivant CNRS Grant CoilChrom (2019–2020), and the LabEx NUMEV (ANR-10-LABX-0020) within the I-SITE MUSE of Montpellier University [No. AAP 2013-2-005, and Flagship Project Gene Expression Modeling (2017–2020)].

### Appendix A: Concentration of ribosomes in the box

We solve Eqs. (16)-(17) in various geometries when  $|\mathbf{r}_\beta - \mathbf{r}_\alpha| > 2r$ .

In  $\mathbb{R}^2$ , we obtain that

$$c(\mathbf{r}) = \begin{cases} c_\infty + \frac{Jr^2}{4D\mathcal{V}} - \frac{J}{4D\mathcal{V}}|\mathbf{r} - \mathbf{r}_\beta|^2 + \frac{Jr^2}{2D\mathcal{V}} \ln\left(\frac{|\mathbf{r} - \mathbf{r}_\alpha|}{r}\right), & |\mathbf{r} - \mathbf{r}_\beta| < r, \\ c_\infty - \frac{Jr^2}{4D\mathcal{V}} + \frac{J}{4D\mathcal{V}}|\mathbf{r} - \mathbf{r}_\alpha|^2 - \frac{Jr^2}{2D\mathcal{V}} \ln\left(\frac{|\mathbf{r} - \mathbf{r}_\beta|}{r}\right), & |\mathbf{r} - \mathbf{r}_\alpha| < r, \\ c_\infty - \frac{Jr^2}{2D\mathcal{V}} \ln\left(\frac{|\mathbf{r} - \mathbf{r}_\beta|}{|\mathbf{r} - \mathbf{r}_\alpha|}\right), & |\mathbf{r} - \mathbf{r}_\alpha| > r, \text{ and } |\mathbf{r} - \mathbf{r}_\beta| > r, \end{cases} \quad (\text{A1})$$

while in  $\mathbb{R}^3$  it holds that

$$c(\mathbf{r}) = \begin{cases} c_\infty + \frac{Jr^2}{2D\mathcal{V}} - \frac{J}{6D\mathcal{V}}|\mathbf{r} - \mathbf{r}_\beta|^2 - \frac{Jr^3}{3D\mathcal{V}} \frac{1}{|\mathbf{r} - \mathbf{r}_\alpha|}, & |\mathbf{r} - \mathbf{r}_\beta| < r, \\ c_\infty - \frac{Jr^2}{2D\mathcal{V}} + \frac{J}{6D\mathcal{V}}|\mathbf{r} - \mathbf{r}_\alpha|^2 + \frac{Jr^3}{3D\mathcal{V}} \frac{1}{|\mathbf{r} - \mathbf{r}_\beta|}, & |\mathbf{r} - \mathbf{r}_\alpha| < r, \\ c_\infty + \frac{Jr^3}{3D\mathcal{V}} \left( \frac{1}{|\mathbf{r} - \mathbf{r}_\beta|} - \frac{1}{|\mathbf{r} - \mathbf{r}_\alpha|} \right), & |\mathbf{r} - \mathbf{r}_\alpha| > r, \text{ and } |\mathbf{r} - \mathbf{r}_\beta| > r. \end{cases} \quad (\text{A2})$$

For a rectangular box of dimensions  $L_x \times L_y$ , we obtain

$$c(\mathbf{r}) = \begin{cases} c_\infty + \frac{Jr^2}{4D\mathcal{V}} - \frac{J}{4D\mathcal{V}}|\mathbf{r} - \mathbf{r}_\beta|^2 + \frac{Jr^2}{2D\mathcal{V}} \ln\left(\frac{|\mathbf{r} - \mathbf{r}_\alpha|}{r}\right) + c_{\mathcal{I}}(\mathbf{r}), & |\mathbf{r} - \mathbf{r}_\beta| < r, \\ c_\infty - \frac{Jr^2}{4D\mathcal{V}} + \frac{J}{4D\mathcal{V}}|\mathbf{r} - \mathbf{r}_\alpha|^2 - \frac{Jr^2}{2D\mathcal{V}} \ln\left(\frac{|\mathbf{r} - \mathbf{r}_\beta|}{r}\right) + c_{\mathcal{I}}(\mathbf{r}), & |\mathbf{r} - \mathbf{r}_\alpha| < r, \\ c_\infty - \frac{Jr^2}{2D\mathcal{V}} \ln\left(\frac{|\mathbf{r} - \mathbf{r}_\beta|}{|\mathbf{r} - \mathbf{r}_\alpha|}\right) + c_{\mathcal{I}}(\mathbf{r}), & |\mathbf{r} - \mathbf{r}_\alpha| > r, \text{ and } |\mathbf{r} - \mathbf{r}_\beta| > r. \end{cases} \quad (\text{A3})$$

where

$$c_{\mathcal{I}}(\mathbf{r}) = \frac{Jr^2}{2D\mathcal{V}} \sum_{j \in \mathcal{N}_\alpha} \ln(|\mathbf{r} - \mathbf{r}_\alpha^{(j)}|) - \frac{Jr^2}{2D\mathcal{V}} \sum_{j \in \mathcal{N}_\beta} \ln(|\mathbf{r} - \mathbf{r}_\beta^{(j)}|), \quad (\text{A4})$$

and where the  $\mathbf{r}_\alpha^{(j)}$  denote the coordinates of the images of the filament initiation site located at  $\mathbf{r}_\alpha$ , and where the  $\mathbf{r}_\beta^{(j)}$  denote the coordinates of the images of the filament termination site  $\mathbf{r}_\beta$ , as illustrated in Figure 3.

Analogously, for a cuboid of dimensions  $L_x \times L_y \times L_z$ , we obtain

$$c(\mathbf{r}) = \begin{cases} c_\infty + \frac{Jr^2}{2D\mathcal{V}} - \frac{J}{6D\mathcal{V}}|\mathbf{r} - \mathbf{r}_\beta|^2 - \frac{Jr^3}{3D\mathcal{V}} \frac{1}{|\mathbf{r} - \mathbf{r}_\alpha|} + c_{\mathcal{I}}(\mathbf{r}), & |\mathbf{r} - \mathbf{r}_\beta| < r, \\ c_\infty - \frac{Jr^2}{2D\mathcal{V}} + \frac{J}{6D\mathcal{V}}|\mathbf{r} - \mathbf{r}_\alpha|^2 + \frac{Jr^3}{3D\mathcal{V}} \frac{1}{|\mathbf{r} - \mathbf{r}_\beta|} + c_{\mathcal{I}}(\mathbf{r}), & |\mathbf{r} - \mathbf{r}_\alpha| < r, \\ c_\infty + \frac{Jr^3}{3D\mathcal{V}} \left( \frac{1}{|\mathbf{r} - \mathbf{r}_\beta|} - \frac{1}{|\mathbf{r} - \mathbf{r}_\alpha|} \right) + c_{\mathcal{I}}(\mathbf{r}), & |\mathbf{r} - \mathbf{r}_\alpha| > r, \text{ and } |\mathbf{r} - \mathbf{r}_\beta| > r, \end{cases} \quad (\text{A5})$$

where

$$c_{\mathcal{I}}(\mathbf{r}) = -\frac{Jr^3}{3D\mathcal{V}} \sum_{j \in \mathcal{N}_\alpha} \frac{1}{|\mathbf{r} - \mathbf{r}_\alpha^{(j)}|} + \frac{Jr^3}{3D\mathcal{V}} \sum_{j \in \mathcal{N}_\beta} \frac{1}{|\mathbf{r} - \mathbf{r}_\beta^{(j)}|}. \quad (\text{A6})$$

- 
- [1] H. Lodish, et al., *Molecular cell biology*, eighth edition, (W.H. Freeman and Company, 2016).
- [2] M. Kosak, *Initiation of translation in prokaryotes and eukaryotes*, *Gene* **234**, 187-208 (1999).
- [3] T. V. Pestova, et al., *Molecular mechanisms of translation initiation in eukaryotes*, *Proceedings of the National Academy of Sciences* **98**, 7029-7036 (2001)
- [4] J. W. B. Hershey, J. N. Sonenberg, and M. B. Mathews, *Principles of translational control: an overview*, *Cold Spring Harbor perspectives in biology* **4**, a011528 (2012).
- [5] P. Shah, Y. Ding, M. Niemczyk, G. Kudla and J. B. Plotkin, *Rate-limiting steps in yeast protein translation*, *Cell* **153**, 1589-1601 (2013).
- [6] T. Chou, *Ribosome recycling, diffusion, and mRNA loop formation in translational regulation*, *Biophysical journal* **85**, 755-773 (2003).
- [7] L. D. Fernandes, P. S. De Moura, and L. Ciandrini, *Gene length as a regulator for ribosome recruitment and protein synthesis: theoretical insights*, *Scientific reports* **7**, 1-11 (2017).
- [8] L. D. Fernandes and L. Ciandrini, *Driven transport on a flexible polymer with particle recycling: A model inspired by transcription and translation*, *Physical Review E* **99**, 052409 (2019).
- [9] S. E. Wells, P. E. Hillner, R. D. Vale and A. B. Sachs, *Circularization of mRNA by eukaryotic translation initiation factors*, *Molecular cell* **2**, 135-140 (1998).
- [10] Q. Vicens, J. S. Kieft, and O. S. Rissland, *Revisiting the closed-loop model and the nature of mRNA 5'-3' communication*, *Molecular cell* **72**, 805-812 (2018).
- [11] R. A. Blythe and M. R. Evans, *Nonequilibrium steady states of matrix-product form: a solver's guide*, *Journal of Physics A: Mathematical and Theoretical* **40**, R333 (2007).
- [12] C. T. MacDonald, J. H. Gibbs, and A. C. Pipkin, *Kinetics of biopolymerization on nucleic acid templates*, *Biopolymer* **6**, 1-5 (1968).
- [13] C. T. MacDonald, and J. H. Gibbs, *Concerning the kinetics of polypeptide synthesis on polyribosomes*, *Biopolymer* **7**, 707 (1969).
- [14] M. C. Romano, M. Thiel, I. Stansfield, and C. Grebogi, *Queueing phase transition: theory of translation*, *Physical review letters* **102**, 198104 (2009).
- [15] P. Bonnin, N. Kern, N.T. Young, I. Stansfield, and M. C. Romano, *Novel mRNA-specific effects of ribosome drop-off on translation rate and polysome profile*, *PLoS computational biology* **13**, e1005555 (2017).
- [16] R. Lipowsky, S. Klumpp and T. M. Nieuwenhuizen, *Random walks of cytoskeletal motors in open and closed compartments*, *Physical Review Letters* **87**, 108101(2001).
- [17] S. Klumpp and R. Lipowsky, *Traffic of molecular motors through tube-like compartments*, *Journal of Statistical Physics* **113**, 233-268 (2003).
- [18] M. J. Müller, S. Klumpp and R. Lipowsky, *Molecular motor traffic in a half-open tube*, *Journal of Physics: Condensed Matter* **17**, S3839 (2005)
- [19] L. Ciandrini, I. Neri, J. C. Walter, O. Dauloudet and A. Parmeggiani, *Motor protein traffic regulation by supplydemand balance of resources*, *Physical Biology* **11**, 056006 (2014).
- [20] I. Neri, N. Kern, and A. Parmeggiani, *Modeling cytoskeletal traffic: an interplay between passive diffusion and active transport*, *New Journal of Physics* **110**, 098102 (2013).
- [21] I. Neri, N. Kern, and A. Parmeggiani, *Exclusion processes on networks as models for cytoskeletal transport*, *New Journal of Physics* **15**, 085005 (2013).
- [22] I. R. Graf, and E. Frey, *Generic transport mechanisms for molecular traffic in cellular protrusions*, *Physical review letters* **118**, 128101 (2017).
- [23] M. Rank, A. Mitra, L. Reese, S. Diez, and E. Frey, *Limited resources induce bistability in microtubule length regulation*, *Physical review letters* **120**, 148101 (2018).
- [24] A. K. Verma, and A. K. Gupta, *Stochastic transport on flexible lattice under limited resources*, *Journal of Statistical Mechanics: Theory and Experiment*, 103210 (2019).
- [25] A. Jindal, A. K. Verma, and A. K. Gupta, *Cooperative dynamics in bidirectional transport on flexible lattice*, *arXiv:2002.09305* (2020).
- [26] T. Chou, K. Mallick, and R. K. P. Zia, *Non-equilibrium statistical mechanics: from a paradigmatic model to biological transport*, *Reports on progress in physics* **74**, 116601(2011).
- [27] D. Chowdhury, *Stochastic mechano-chemical kinetics of molecular motors: a multidisciplinary enterprise from a physicists perspective*, *Physics Reports* **529**, 1-197 (2013).
- [28] C. U. T. Hellen, and P. Sarnow, *Internal ribosome entry sites in eukaryotic mRNA molecules*, *Genes & development* **15**, 1593-1612 (2001).
- [29] J. L. Woolford, and S. J. Baserga, *Ribosome biogenesis in the yeast *Saccharomyces cerevisiae**, *Genetics* **195**, 643-681 (2013).
- [30] J. R. Warner, *The economics of ribosome biosynthesis in yeast*, *Trends in biochemical sciences* **24**, 437-440 (1999).
- [31] R. P. Joyner, et al., *A glucose-starvation response regulates the diffusion of macromolecules*, *Elife* **5**, e09376 (2016).

- [32] M. C. Munder, et al., *A pH-driven transition of the cytoplasm from a fluid-to a solid-like state promotes entry into dormancy*, *Elife* **5**, e09347 (2016).
- [33] V. L. MacKay, et al., *Gene expression analyzed by high-resolution state array analysis and quantitative proteomics: response of yeast to mating pheromone*, *Molecular & Cellular Proteomics* **3**, 478-489 (2004).
- [34] A. Biever, et al., *Monosomes actively translate synaptic mRNAs in neuronal processes* **367**, 6477 (2020).
- [35] O. Dauloudet, *Étude théorique des phénomènes de transport intracellulaire hors-équilibre thermodynamique: rôle du couplage entre transport actif et diffusif en volume confiné*, PhD diss., Montpellier University 2015.
- [36] B. Derrida, E. Domany, and D. Mukamel, *An exact solution of a one-dimensional asymmetric exclusion model with open boundaries*, *Journal of Statistical Physics* **69**, 667-687 (1992).
- [37] R. Milo and R. Phillips, *Cell biology by the numbers*, (Garland Science (2016)).
- [38] J. Guo, X. Lian, J. Zhong, T. Wang, and G. Zhang, *Length-dependent translation initiation benefits the functional proteome of human cells*, *Mol Biosyst* **11**, 370-378 (2015).
- [39] U. Alon, *An Introduction to Systems Biology: Design Principles of Biological Circuits* [Chapman & Hall/CRC (2007)].
- [40] J. Jeon, et al., *In vivo anomalous diffusion and weak ergodicity breaking of lipid granules*, *Physical review letters* **106**, 048103 (2011).
- [41] V. Tejedor, et al., *Quantitative analysis of single particle trajectories: mean maximal excursion method*, *Biophysical journal* **98**, 1364-1372 (2010).
- [42] F. Höfling, and T. Franosch, *Anomalous transport in the crowded world of biological cells*, *Reports on Progress in Physics* **76**, 046602 (2013).
- [43] A. Sanamrad, et al., *Single-particle tracking reveals that free ribosomal subunits are not excluded from the Escherichia coli nucleoid*, *Proceedings of the National Academy of Sciences* **111**, 11413-11418 (2014).
- [44] R. Young, and H. Bremer, *Polypeptide-chain-elongation rate in Escherichia coli B/r as a function of growth rate*, *Biochemical Journal* **160**, 185-194 (1976).
- [45] N. Bilgin, F. Claesens, H. Pahverk, and M. Ehrenberg, *Kinetic properties of Escherichia coli ribosomes with altered forms of S12*, *Journal of molecular biology* **224**, 1011-1027 (1992).
- [46] S. Proshkin, A. R. Rahmouni, A. Mironov, and E. Nudler, *Cooperation between translating ribosomes and RNA polymerase in transcription elongation*, *Science* **328** 504-508 (2010).
- [47] J. Forchhammer, and L. Lindahl, *Growth rate of polypeptide chains as a function of the cell growth rate in a mutant of Escherichia coli*, *J Mol Biol* **55**, 563-568 (1971).
- [48] L. Ciandrini, I. Stansfield, M. C. Romano, *Ribosome traffic on mRNAs maps to gene ontology: genome-wide quantification of translation initiation rates and polysome size regulation*, *PLoS computational biology* **9**, 1 (2013).
- [49] J. C. Ritland Politz, R. A. Tuft, and T. Pederson, *Diffusion-based transport of nascent ribosomes in the nucleus*, *Molecular biology of the cell* **14**, 4805-4812 (2003).
- [50] Y. Arava, Y. Wang, J. D. Storey, C. L. Liu, P. O. Brown, and D. Herschlag, *Genome-wide analysis of mRNA translation profiles in Saccharomyces*, *Proc. Natl. Acad. Sci. USA* **100**, 3889-3894 (2003).
- [51] M. Siwiak, and P. Zielenkiewicz, *A comprehensive, quantitative, and genome-wide model of translation*, *PLoS Comput. Biol.* **6**, e1000865 (2010).
- [52] T. von der Haar, *A quantitative estimation of the global translational activity in logarithmically growing yeast cells*, *BMC Syst. Biol.* **2**, 87 (2008).
- [53] D. T. Gillespie, *A general method for numerically simulating the stochastic time evolution of coupled chemical reactions*, *J. Comput. Phys.* **22**, 403-34 (1976); Gillespie D. T., *Exact stochastic simulation of coupled chemical reactions*, *The Journal of Physical Chemistry* **81**, 2340-61 (1977).
- [54] M. Newman, and G. Barkema, *Monte carlo methods in statistical physics*, (Oxford University Press: New York, 1999).
- [55] Walter J.-C., and Barkema G. T., *An introduction to Monte Carlo methods*, *Physica A* **418**, 78-87, Lecture Notes of the 13th International Summer School: Fundamental Problems in Statistical Physics (Leuven, Belgium, 16-29 June 2013).
- [56] Bressloff, Paul C., and Jay M. Newby. "Stochastic models of intracellular transport." *Reviews of Modern Physics* 85.1 (2013): 135.
- [57] Jackson, John D. (1999). *Classical Electrodynamics* (3rd ed.). New York: John Wiley & Sons.
- [58] Richard P. Feynman, Robert B. Leighton, Matthew Sands, *The Feynman Lectures on Physics: Mainly Electromagnetism and Matter, Volume 2* (1977).
- [59] B. Derrida, E. Domany, and D. Mukamel. An exact solution of a one-dimensional asymmetric exclusion model with open boundaries. *Journal of Statistical Physics*, 69(Nos. 3/4), 1992.
- [60] Anatoly B. Kolomeisky, Gunter M. Schütz, Eugene B Kolomeisky, and Joseph P Straley. Phase diagram of one-dimensional driven lattice gases with open boundaries. *J. Phys. A : Math. Gen.*, 31 :69116919, 1998.
- [61] Parmeggiani, A. (2009). Non-equilibrium collective transport on molecular highways. In *Traffic and Granular Flow07* (pp. 667-677). Springer, Berlin, Heidelberg.
- [62] Cook, L. Jonathan, and R. K. P. Zia. "Feedback and fluctuations in a totally asymmetric simple exclusion process with finite resources." *Journal of Statistical Mechanics: Theory and Experiment* 2009.02 (2009): P02012.